Near Surface Geophysics, 2007, 183-194

An experiment of non-invasive characterization of the vadose zone via water injection and cross-hole time-lapse geophysical monitoring

Rita Deiana[1], Giorgio Cassiani[*,2], Andreas Kemna[3], Alberto Villa[1], Vittorio Bruno[1] and Andrea Bagliani[1]

[1]*Dipartimento di Scienze Geologiche e Geotecnologie, Università di Milano Bicocca, Italy*
[2]*Dipartimento de Geoscienze, Università di Padova, Italy*
[3]*Institute of Chemistry and Dynamics of the Geosphere, Forschungszentrum Jülich GmbH, Germany*

Received July 2006, revision accepted November 2006

ABSTRACT

The characterization of the vadose zone, i.e. the part of the subsurface above the water table, is a challenging task. This zone is difficult to access with direct methods without causing major disturbance to the natural *in-situ* conditions. Hence the increasing use of geophysical methods capable of imaging the water presence in the vadose zone, such as ground-penetrating radar (GPR) and electrical resistivity tomography (ERT). This type of monitoring can be applied both to processes of natural infiltration and to artificial injection (tracer) tests, by collecting multiple data sets through time (time-lapse mode). We present the results of a water-injection experiment conducted at a test site in Gorgonzola, east of Milan (Italy). The site is characterized by Quaternary sand and gravel sediments that house an extensive unconfined aquifer, potentially subject to pollution from industrial and agricultural sources. ERT and GPR profiles were acquired in 2D cross-hole configuration and time-lapse mode over a period of several days preceding and following the injection of 3.5 m^3 of fresh water in a purpose-excavated trench. A 3D model of the water-infiltration experiment was calibrated against the time-lapse cross-hole data, particularly focusing on the ability of the model to reproduce the vertical motion of the centre of mass of the injected water as imaged by GPR and ERT. This model calibration provided an estimate of the isotropic hydraulic conductivity of the sediments in the range of 5–10 m/d. However, all isotropic models overpredict the measured excess of moisture content, caused by water injection, as imaged by GPR. The calibration of anisotropic models for the vertical hydraulic conductivity, with the horizontal hydraulic conductivity determined by direct measurement, also leads to a good fit of the sinking of the centre of mass, with a better mass balance in comparison with field data. The information derived from the experiment is key to a quantitative assessment of aquifer vulnerability to pollutants infiltrating from the surface.

1 INTRODUCTION

The presence and flow of water in the vadose (or unsaturated) zone controls a number of phenomena of great environmental interest, such as contamination of groundwater resources, catchment hydrology, flood generation and slope stability. Unfortunately, vadose zone hydrology is characterized by a complex, non-linear behaviour, controlled by gravity and capillary forces. Soil water content can have large spatial variations both in the vertical and in the horizontal directions (e.g. Flury *et al*. 1994). In addition, the hydrological characterization of the vadose zone is technically challenging, particularly when the investigation extends deeper than one or two metres below ground. Direct measurement of water content requires the recovery of soil samples for laboratory analyses. These direct measurements are invasive, based on drilling, and consequently can cause major disturbance to the natural *in-situ* conditions, particularly moisture content. This fact has led to the increasing use of non-invasive, geophysical methods, particularly ground-penetrating radar (GPR) and electrical resistivity tomography (ERT), often in a cross-borehole configuration, to investigate the vadose zone (Slater *et al.* 1997; *Binley et al*. 2001, 2002a; Alumbaugh *et al*. 2002; Cassiani, Strobbia and Gallotti 2004; for reviews see Huisman *et al*. 2003 and Cassiani, Binley and Ferré 2006a).

From a practical standpoint, two compartments can be identi-

* giorgio.cassiani@unipd.it

fied in the unsaturated zone that can be imaged using different geophysical techniques. The *shallow* vadose zone, no deeper than a few metres below ground, can be successfully imaged, with extensive spatial coverage, by taking measurements from the ground surface (e.g. van Overmeeren, Sarrowan and Gehrels 1997; Huisman *et al*. 2001, 2002; Grote, Hubbard and Rubin 2003; Cassiani *et al.* 2006b). In contrast, the *deep* vadose zone requires measurements in single boreholes, between boreholes, or from the surface to boreholes in order to achieve sufficient resolution for quantitative hydrological interpretation (e.g. Binley *et al*. 2002b; Cassiani *et al*. 2004; Cassiani and Binley 2005).

In most cases the ultimate goal is the identification of hydraulic parameters of the vadose zone. Some authors (e.g. Slater and Lesmes 2002; Lesmes and Friedman 2005) have shown that, using suitable petrophysical relationships between geophysical and hydrological parameters, hydraulic structures could be derived directly, at least in the laboratory. However, accurate petrophysical relationships linking geophysical and hydrological properties directly are rarely available for the site of interest, and a more indirect approach based on model calibration is often necessary, as shown in this paper and by previous work (e.g. Binley *et al.* 2002b; Cassiani and Binley 2005). The dependence of the geophysical response on changes in soil moisture content, e.g. via changes in electrical resistivity or dielectric properties, is the key mechanism that permits the use of non-invasive techniques to monitor the vadose zone in time-lapse mode, i.e. via repeated measurements over time. The use of these techniques in different configurations in the shallow and deep vadose zones can provide high-resolution images of hydrogeological structures and, in some cases, a detailed assessment of dynamic processes in the subsurface environment. Both natural infiltration processes and specifically designed tracer tests can be monitored over periods of time that can last from a few hours to several years. The data from non-invasive techniques can subsequently be used to calibrate physical-mathematical models of water flow in the unsaturated zone (Fig. 1).

The objectives of this study are:

1 To describe and discuss the time-lapse geophysical data acquired during a water-injection experiment in the vadose zone, conducted in Quaternary sediments of the Po River plain; the high hydraulic conductivity of these sediments require the experiment to be monitored in time-lapse at a very high frequency, unlike previous work (e.g. Binley *et al.* 2002b).
2 To assess the value of such data in the calibration of an unsaturated flow model describing the experiment, with the aim of estimating unsaturated hydraulic parameters at field scale.

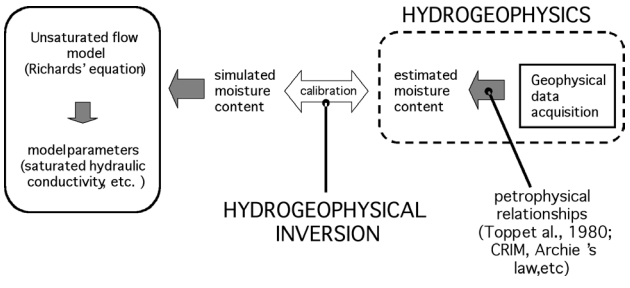

FIGURE 1
A conceptual scheme for the use of geophysical data to calibrate unsaturated water flow models (re-drawn from Cassiani *et al.* 2006a).

2 METHODOLOGY

Non-invasive monitoring of the vadose zone can be successfully conducted using GPR and ERT; both methods underwent rapid development in the 1980s and 1990s. However, successful application of these technologies, borehole-to-borehole, still requires attention and specific tuning to the desired goals of the survey. In the following, we discuss some of the aspects relevant to time-lapse monitoring of the vadose zone.

2.1 Cross-hole electrical resistivity tomography (ERT)

Since the early 1980s, ERT has been used both in the laboratory and in the field to study hydrological properties of soils and rocks, especially by injecting a tracer (generally water in the vadose zone and saline water in the saturated zone) and monitoring the evolution of resistivity images in time-lapse. A number of successful case studies have been reported in the literature (e.g. Binley, Henry-Poulter and Shaw 1996; Slater *et al*. 1997, 2000, 2002; Kemna *et al*. 2002; Singha and Gorelick 2005; Vanderborght *et al*. 2005; Cassiani *et al.* 2006c). The bulk electrical resistivity of a rock sample increases with increasing electrical resistivity of the saturating fluid and with decreasing saturation of the conducting fluid, according to Archie's law [1942]. This relationship, between electrical resistivity and volumetric moisture content, offers data suitable for parametrizing and constraining models of groundwater flow in the unsaturated zone.

The classical approach using surface resistivity imaging is rarely applied to the study of vadose-zone processes deeper than a few metres because of the limited sensitivity at depth. Park (1998) is one of the few published studies that use surface arrays to examine flow in the unsaturated zone at a depth of over 10 m, albeit under forced loading. In order to enhance sensitivity at depth, electrodes may be installed in boreholes. For example, Binley *et al.* (2002a) demonstrated how borehole-based electrode arrays may be used to characterize seasonal variation in volumetric water content to depths of 10 m over a period of over two years at a sandstone site in the UK. Single-borehole arrays have limited lateral coverage, however, and electrode arrays may be utilized using cross-borehole electrical resistivity tomography to obtain high-resolution images of resistivity at depth. Cross-borehole resistivity is an extension of conventional surface resistivity imaging and uses similar inverse modelling techniques (see Daily *et al.* 2004a).

Daily *et al.* (1992) gave the first demonstration of how borehole ERT can be applied to the study of water flow in the deep vadose zone. Other vadose-zone studies using cross-borehole ERT include, among others, Ramirez *et al*. (1996), Slater *et al.*

(1997), Zaidman *et al*. (1999), Binley *et al.* (2002b), French *et al.* (2002) and Daily, Ramirez and Binley (2004b).

As pointed out by Binley and Kemna (2005), the main advantages of cross-borehole resistivity imaging, in comparison with surface resistivity imaging, are that: (1) high resolution at depth is possible and (2) investigations can be made without the need for surface access (for example, surveys under buildings are possible). However, the method suffers from a number of disadvantages: (1) boreholes are required (which often need to be purpose-drilled) and good contact between electrodes and formation is not easily achieved; (2) the boreholes must not be too far apart otherwise sensitivity is reduced; (3) data acquisition often requires more sophisticated installation and is often more time consuming than for surface ERT; (4) data noise levels are usually higher than those using surface electrodes; (5) data processing techniques are more complex. In recent years, sophisticated ERT inversion techniques have been developed, making tomographic imaging of subsurface fluid movement possible. The most commonly used method was proposed by Daily *et al.* (1992) and LaBrecque *et al.* (1996) and is known as Occam's inversion, originally named by Constable, Parker and Constable (1987) (for other applications): regularization is performed by seeking the 'smoothest' model compatible with the error level in the data. This error level is generally estimated by comparing the measured data with their reciprocals (interchanging potential with current electrodes). While this procedure doubles the acquisition time, it is necessary in order to yield an objective assessment of data quality and the consequent resolution achievable with a given data set. More details on ERT inversion and particularly on Occam's approach can be found in Kemna (2000), Binley and Kemna (2005), Daily *et al.* (2004a,b, 2005).

When time-lapse measurements are performed, changes in ERT images with time can be assessed by simply carrying out independent data inversions, each representing a snapshot at one time during the process. By subtraction of pixel-by-pixel values from some background image, changes are easily computed. However, in most cases, changes over time are small relative to the natural spatial variability within the region of interest. In addition, when using 2D acquisition and inversion while monitoring 3D processes, such as a tracer injection, off-plane changes may induce a considerable level of data error that changes over time. Consequently, pixel-by-pixel subtraction may prove ineffective in providing clear images of tracer motion with time. In order to overcome these difficulties, the analysis of the resistivity variations with time can be performed following the method of Daily *et al.* (1992), which uses the ratio of the resistance measured at the same quadripole at different times. Thus, for each quadripole, the data to be inverted at each time step following the first one are derived as the ratio between current and background resistance values (e.g. Cassiani *et al.* 2006c). Alternatively, LaBrecque and Yang (2000) proposed a generalization of this procedure, called 'difference inversion', where the restriction of a homogeneous reference model is dropped. Smoothness is imposed directly on the time-lapse model change. The result of the difference inversion is resistivity images that show the percentage variation of resistivity and consequently, for instance, the qualitative or quantitative change in the moisture content of the soil. This approach can be considered to be more generally applicable than the ratio inversion and has been successfully used for tracer test monitoring (e.g. Kemna *et al.* 2002).

Even though flow and transport processes in the vadose zone can be successfully monitored and imaged using time-lapse cross-borehole ERT, a number of important limitations must be kept in mind when interpreting cross-hole ERT images of the vadose zone. First, regularization is necessary in order to constrain the number of possible solutions to the non-unique ERT inverse problem. The choice of regularization method is not defined by the data, but is instead based on *a-priori* information and, generally, on experience. The images obtained depend strongly on the selected regularization, leading to potential mis-interpretation of the results (Binley *et al*. 2002b). Note that either isotropic or anisotropic regularization can be applied with potentially different results (see e.g. Kemna *et al.* 2002). Second, for cross-hole electrode arrangements, data sampling and spatial resolution are markedly enhanced in the vertical compared to the horizontal direction, and consequently different regions in the inverted image have substantially different resolution, with important consequencies especially if a quantitative characterization is sought (Day-Lewis, Singha and Binley 2005). Third, the relationship between bulk subsurface electrical conductivity, as reflected by the ERT data, and tracer concentration depends on various textural and physico-chemical properties of the soil/rock-groundwater system. These properties are generally site-dependent, with significant consequences for quantitative data analysis.

2.2 Cross-hole ground-penetrating radar (GPR)

Ground-penetrating radar is a very effective technology for probing the near subsurface, especially for environmental and engineering applications. More specifically, GPR is particularly suitable for hydrological investigations (Annan 2005) because of the direct link between propagation velocity and soil volumetric moisture content; consequently, GPR is of direct interest for studies of the vadose zone (e.g. Hubbard *et al*. 1997; Eppstein and Dougherty 1998; Alumbaugh *et al.* 2002). The GPR propagation velocity is inversely proportional to the soil bulk dielectric constant k through the simple relationship,

$$v = \frac{c}{\sqrt{k}}, \tag{1}$$

where c is the electromagnetic wave velocity in the free space (0.3 m/ns) and k is the effective dielectric constant, which in turn can be related to the volumetric moisture content of the soil by means of suitable petrophysical relationships (for a review see Chelidze and Guéguen 1999). Two empirical approaches have gained popularity in practical applications: one is the complex refractive index method (CRIM), which is

a volume-averaging relationship and explicitly incorporates porosity, volumetric water content, and the dielectric constant of solid matrix, air and water phases (Roth *et al*. 1990; Chan and Knight 1999). A second empirical approach was developed for the interpretation of time-domain refractometry data. Topp *et al*. (1980) used a large set of different soils to develop an empirical relationship to relate the effective permittivity to the volumetric water content, which takes no explicit account of variations in the properties of the solid matrix (e.g. permittivity, porosity, connectivity, etc.):

$$\theta = -5.3\times10^{-2} + 2.92\times10^{-2}\kappa - 5.5\times10^{-4}\kappa^2 + 4.3\times10^{-6}\kappa^3 . \quad (2)$$

The Topp model is generally applied unless the medium has properties (e.g. porosity, magnetic susceptibility, high clay content) that differ from typical agricultural soils.

As GPR energy propagation is significantly limited by the presence of conducting soil layers, in order to achieve sufficient penetration and resolution at depth it is often necessary to deploy GPR antennae in boreholes. Borehole transmission surveys may be conducted in three different antenna configurations, depending on the survey goals and practical constraints, in order to determine dielectric properties at the field scale. In two modes, a GPR signal is transmitted from one antenna placed in the first borehole and is received by a second antenna in the other borehole. Measurement of the received electromagnetic wave permits determination of the first arrival and hence the velocity v of the wave. For multi-offset-gather surveys, the receiver is moved to different locations in one borehole whilst the transmitter remains fixed. The transmitter is then moved, the process is repeated and the measurements are recorded at an array of receiver positions for each of the transmitter positions. Following collection of all data in this mode and determination of the traveltime for each wavepath-line, it is possible to derive a tomogram of velocity within the plane of the borehole pair. In contrast, a zero-offset-profile configuration may be determined by keeping the transmitter and the receiver at the same depth. In this way, only measurements at successive depths are collected. By systematically lowering or raising the pair of antennas in the two boreholes, it is possible to build a 1D profile of average inter-borehole traveltime over the entire borehole length. If only one borehole is available, a profile of cumulative traveltime to a given depth can be obtained by laying the transmitter antenna on the ground surface next to the borehole and lowering the receiver antenna to progressively greater depths (vertical radar profiling).

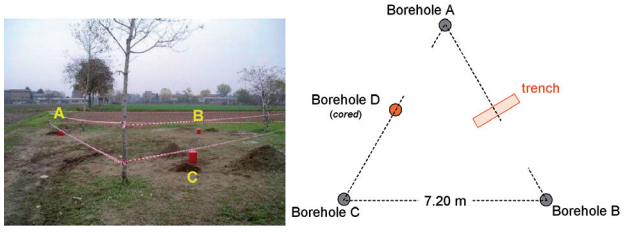

FIGURE 2
Scheme of the Gorgonzola experimental site.

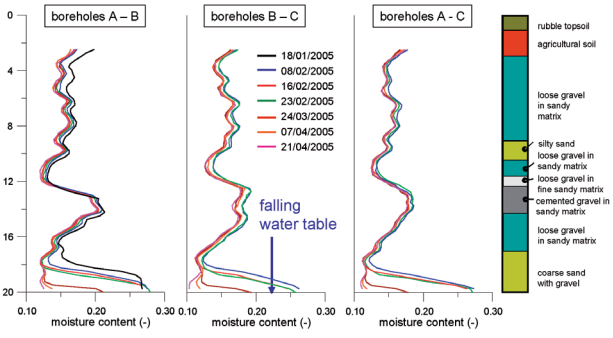

FIGURE 3
Moisture content profiles estimated at the Gorgonzola test site from January 2005 to April 2005, derived from zero-offset-profile GPR and the constitutive relationship of Topp *et al.* (1980).

Each of the three transmission modes considered has advantages and disadvantages. Multi-offset gathers have the greatest information content, and can represent the actual (albeit 2D) distribution of dielectric properties. However, at least with currently available borehole GPR systems, acquisition is slow and cumbersome, and may require many hours for each pair of holes. In addition, tomographic inversion is required to reconstruct the velocity image. Zero-offset-profiles are fast to acquire and easy to interpret, but only provide 1D information. Both multi-offset gathers and zero-offset profiles require two closely spaced and parallel boreholes (generally less than 10 m apart even under ideal conditions) with plastic casing.

3 THE GORGONZOLA FIELD SITE

3.1 Site description

Time-lapse cross-hole ERT and GPR measurements were used to monitor a water-injection experiment at the Gorgonzola experimental site, located a few km east of Milan, Italy. The field site is located near an industrial area; therefore, the aquifer is potentially threatened by pollution coming from the land surface. The site has four boreholes (Fig. 2) to monitor the unsaturated flow dynamics in the local alluvial Quaternary sediments of the Po River plain, characterized by a fairly coarse sandy-gravel grain-size distribution. The boreholes extend to a depth of about 20 m, i.e. below the water table for most of the year. Three boreholes (A, B, C, in Fig. 2) are permanently equipped with a set of 24 stainless-steel borehole electrodes for ERT imaging, spaced vertically at intervals of 0.8 m, between 2 m and 20 m depth. Contact with the surrounding formation, which consists of loose to poorly cemented sand and gravel, was achieved by backfilling the boreholes with a mixture of drilling cuts and concrete powder between 2 m and 15 m depth. A gravel pack was placed around the slotted section, between 15 and 20 m depth, to ensure that the

changing elevation of the water table could be measured all year round. Because of the irrigation in the surrounding countryside, the water table has a yearly oscillation of between 13.5 m and 20 m below ground level.

Analysis of a soil core extracted from a fourth borehole in July 2005 (D in Fig. 2) gave better knowledge of the site stratigraphy (Fig. 3). Several features can be noted that have a direct impact on the site's hydrology: (a) the presence of a 3-m-thick surface layer composed of rubble and agricultural soil, partly over-consolidated by construction operations at the nearby parking lot (this layer is present only locally and consequently is of no interest in terms of characterization of the vadose zone in the area); (b) a prevalence of Quaternary sand/gravel sediments of fluvial/glacial origin, which is highly permeable; (c) the existence of a 2-m-thick layer of cemented gravel and sand at roughly 12 m depth.

During drilling of the cored borehole D, a Lefranc permeability test was performed at a depth of 6 m. The resulting field-saturated hydraulic conductivity value was 36 m/d. Given the test characteristics, this value corresponds to an estimate of the horizontal hydraulic conductivity.

The three ERT boreholes were installed in October 2004. Starting in January 2005, monitoring of *in-situ* moisture-content conditions was performed on three borehole pairs (A-B, A-C and B-C) using cross-hole ERT and GPR (both in zero-offset profile and multi-offset modes) with the same instrumentation and data acquisition adopted later in the water injection experiment (see sections below). The results of the GPR zero-offset-profile monitoring from January to April 2005, converted to moisture content estimations using the Topp *et al*. (1980) relationship, are shown in Fig. 3 for the three pairs of boreholes. There are very strong similarities between the three independent data sets, confirming that the site has a layered structure. The cemented sand/gravel layer at 12–14 m depth is very noticeable in Fig. 3. This layer seems capable of holding substantially more water than the surrounding non-cemented material. This is probably due to the higher residual water content of the cement, and possibly also to its lower permeability.

Disregarding the falling water table, which is imaged very accurately, compared with direct water-table measurements in the boreholes, very little variation in moisture content is noticeable over time. We can therefore conclude that the site undergoes very small changes in saturation conditions under natural infiltration, which is probably strongly limited by the allochthonous soil layer on top. Under quasi-steady-state conditions, it is impossible to identify uniquely the unsaturated flow parameters of the vadose zone (Cassiani and Binley 2005). In order to obtain transient, more informative conditions, a water-injection test was planned and performed at the site.

3.2 Water injection test and geophysical monitoring

In July 2005, an artificial water-injection experiment was performed using a 2-m-deep, 2.60-m-long trench dug perpendicular to the plane described by boreholes A and B, which are located 6.65 m apart (Fig. 2). A total of 3.5 m^3 of tap water was injected into the trench over a period of about 2 hours by pouring the water directly into the trench (Fig. 4). The evolution of the injected water plume in space and time was monitored by ERT and GPR measurements for a total of 93 hours, from July 5 (date of water injection) to July 11, 2005. ERT data were acquired between boreholes A and B, i.e. corresponding to the symmetry plane crossing the trench, using an IRIS Syscal Pro system with 10 physical channels and 48 multiplexed channels. The acquisition was based on a dipole-dipole measurement scheme built as a mixture of AB-MN and AM-BN schemes (see Binley and Kemna 2005), in order to benefit from both the good resolution of the AB-MN scheme (where current and potential dipoles are of small size with both electrodes of the same type in the same borehole) and the good signal/noise ratio of the AM-BN scheme. The data were of good quality, thus this latter scheme (advocated e.g. by Bing and Greenhalgh 2000) proved practically redundant in this case. In addition to the borehole electrodes, eight electrodes were placed on the ground surface along the line connecting boreholes A and B, at 0.9 m spacing. These electrodes are necessary to attain sufficient coverage in the upper part of the A-B section, where injection (the trench) takes place. In order to accommodate these surface electrodes in the 48-channel capability of the instrument, eight borehole electrodes (the six deepest and two with poor contact) were sacrificed and removed from the measurement scheme. A total of 3168 measurements were taken for each ERT image, including direct and reciprocal configurations. The total time required for each acquisition, optimizing the use of the 10 physical channels of the IRIS Syscal Pro, was about 20 minutes.

The same boreholes (A and B) could also be used for cross-hole GPR tomography. Our field experience demonstrated that, in spite of the existence of electrodes and cables in each borehole, it was possible to acquire good-quality data. At this site, we noticed that spurious arrivals arose when the vertical offset

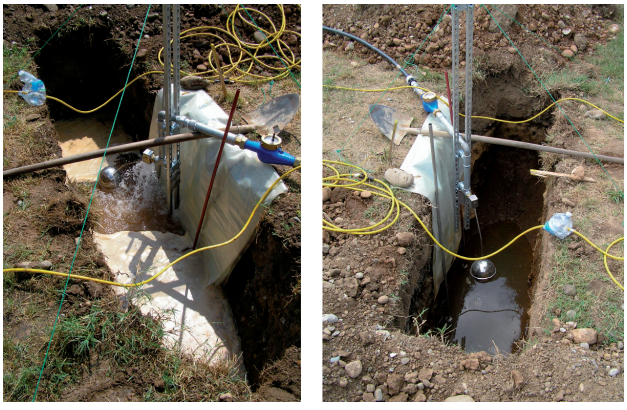

FIGURE 4
Water injection in the purpose-dug trench at the Gorgonzola site, July 2005.

between transmitter and receiver antennae exceeded an angle of 45°. This problem prevented us from using vertical radar profiling at this site, and is also in partial contrast with the need for good multi-angle coverage in multi-offset-gather data. At present we are unable to attribute the problem to the existence of cables in the boreholes, as similar problems have been noticed in boreholes without cables and electrodes (Peterson 2001; Alumbaugh *et al.* 2002). A cause of this limitation in cross-hole GPR may be related to first-arrival energy travelling between antenna tips rather than antenna centres (Irving and Knight 2005), but at present the issue is still being debated.

At the Gorgonzola site, both multi-offset-gather and zero-offset-profile surveys were repeatedly acquired before, during and after water injection. A PulseEkko 100 system was used with 100-MHz borehole antennae. In zero-offset-profile surveys, antennae were lowered with 0.25 m vertical spacing. For multi-offset gathers, a coarser 0.5 m spacing was selected in order to minimize the acquisition time. For the same reason, multi-offset-gather surveys extended only to a depth of 14.75 m, and not to the bottom of the boreholes. The depth of multi-offset-gather investigation is sufficient to image the 3.5 m^3 water injection, as confirmed by zero-offset-profile monitoring that extends to the borehole bottom (see next section). The acquisition parameters (number of stacks, time sampling) were selected to minimize the acquisition time for each shot and still preserve the data quality. In spite of all such efforts, the acquisition time for multi-offset gathers still amounted to about 1 hr for each survey.

Before water injection began, ERT, GPR multi-offset-gather and GPR zero-offset-profile background measurements were made. Figure 5 shows the background-reference images for ERT and GPR multi-offset gathers. In the background ERT image, note the presence of a conductive layer centred around 2 m depth, corresponding to the over-consolidated agricultural soil detected in the core, while the trench location appears as a high-resistivity anomaly at the surface, midway between the boreholes.

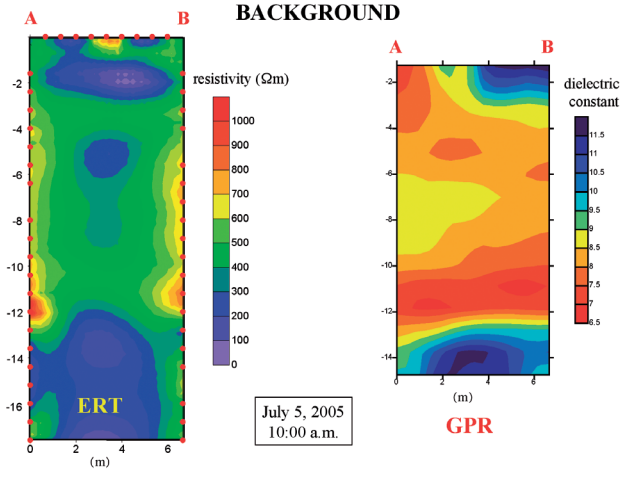

FIGURE 5

Resistivity and dielectric constant background (i.e. before water injection) as derived respectively from ERT and multi-offset-gather GPR cross-hole imaging. The left-hand panel shows the location of active electrodes as red dots. Note the presence of a conductive layer approximately 2 m below ground and the trench location that appears as a high-resistivity anomaly at the top.

Both ERT and multi-offset-gather images confirm the presence of a layer having lower electrical conductivity and higher dielectric constant at a depth of about 12 m. This layer is wetter than the surrounding material, and corresponds to the 2 m thick layer of cemented gravel and sand detected by the drilling core in borehole D. The bottom of this wetter layer cannot be imaged by multi-offset gathers because the acquisition extends only to 14.75 m depth. Since during the experiment the water table was at a depth of approximately 15.50 m below ground (shallower than shown in the zero-offset profiles shown in Fig. 3), the bottom of this cemented layer is also difficult to detect in ERT images, where it is combined with the low resistivity of the nearby saturated zone.

3.3 Results of geophysical time-lapse monitoring

ERT inversion

Inversion of ERT data was performed using the CRTomo 2D code (Kemna 2000). This code also allows for the difference inversion of time-lapse data (see section 2.1 and LaBrecque and Yang 2000). The vertical plane defined by boreholes A and B was discretized into a grid of 56 cells in the *x*-direction and 35 cells the in *y*-direction, also accommodating outer padding regions (allowing for the flow of current away from the inter-borehole region) of relatively limited extent, thanks to the third-type boundary conditions defined at the lower and lateral grid boundaries. For the absolute images, such as the pre-injection background, the reciprocal analysis was set to exclude data that exceeded a 10% reciprocal error level, and the inversion target was set accordingly. For difference inversion, the error analysis cannot be conducted on the basis of the reciprocals and tighter error levels are generally adopted. In our case, error levels in the range 2–5% were investigated, and a 2% error level was finally chosen for all difference inversions. In all cases isotropic regularization was used. Conversion from resistivity images into moisture content has so far not been attempted: estimates of Archie's law parameters from core data are in progress

GPR zero-offset-profile and multi-offset-gather inversion

GPR data analysis was limited to traveltime picking and inversion for velocity distribution, to obtain images of the dielectric constant and, by conversion using the model of moisture content images (equation (2)) of Topp *et al.* (1980).

Zero-offset profiles were analysed under the assumption of straight-ray horizontal propagation. While this approach is known to introduce possible errors due to critically refracted waves, the proposed corrections (e.g. Rucker and Ferré 2004) rely on the hypothesis that layers with sharp velocity changes can be identified. This is not always the case, and we did not

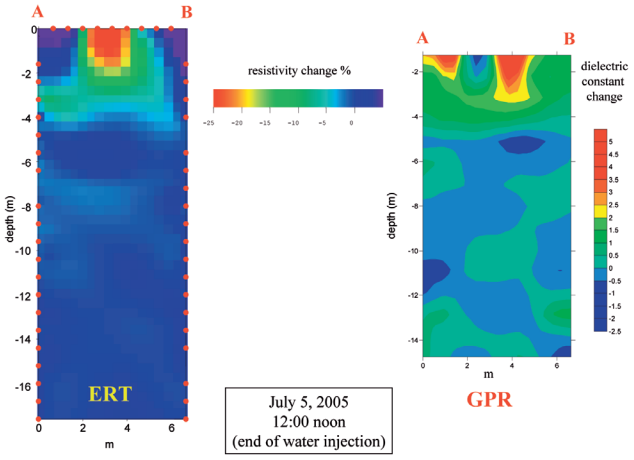

FIGURE 6
Resistivity and dielectric constant changes with respect to background (i.e. before water injection; see Fig. 5) at the end of water injection.

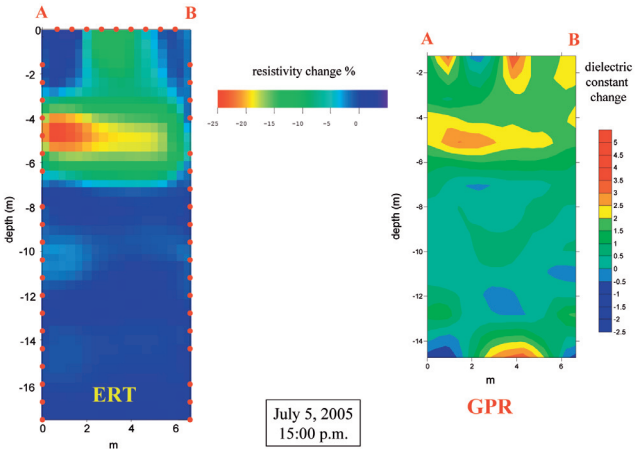

FIGURE 7
Resistivity and dielectric constant changes with respect to background (i.e. before water injection; see Fig. 5) three hours after the start of water injection.

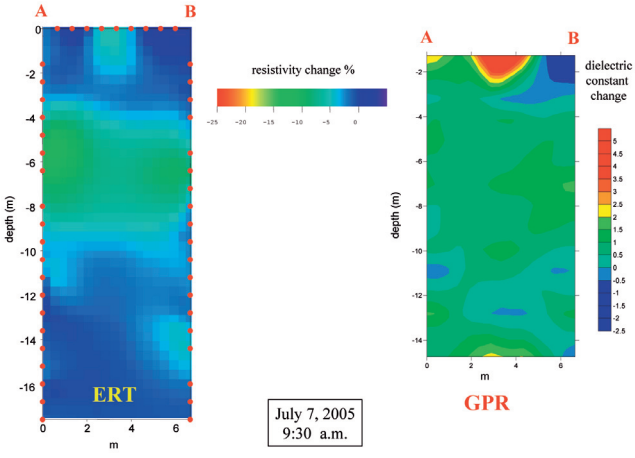

FIGURE 8
Resistivity and dielectric constant changes with respect to background (i.e. before water injection; see Fig. 5) about 22 hours after the start of water injection.

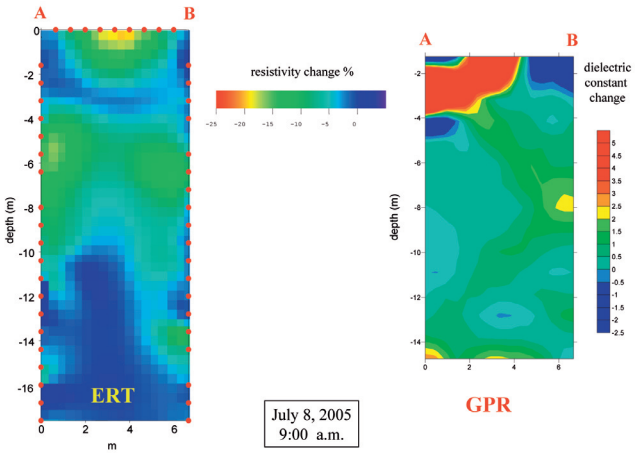

FIGURE 9
Resistivity and dielectric constant changes with respect to background (i.e. before water injection; see Fig. 5) about 46 hours after the start of water injection.

want to make this strong hypothesis. The straight-ray assumption was also adopted for the tomographic inversion of multi-offset-gather data, which was performed using the Migratom code (Jackson and Tweeton 1994). For both zero-offset-profile and multi-offset-gather data, time-lapse analysis was based purely on differences in the individual inverted images.

Results of ERT and GPR monitoring

Figures 6–9 show the results of ERT difference inversion, in terms of percentage resistivity change, and of GPR multi-offset-gather inversion, in terms of changes in dielectric constant obtained from differences of individual inverted images. ERT and multi-offset-gather images are consistent with each other and show very clearly the infiltrating water front from the trench (Fig. 6) and its migration deeper into the unsaturated zone only three hours later (Fig. 7), confirming that the sediments are highly permeable and that the infiltration process is very fast. In spite of the different resolution characteristics of ERT and GPR multi-offset gathers (as discussed e.g. by Day-Lewis and Lane 2004; Day-Lewis *et al.* 2005), the images are very similar (consider e.g. Fig. 7), thus confirming that the observed features are true signal, induced by the water injection. ERT and GPR multi-offset gathers consistently show some lateral spread of the infiltrating slug.

Figure 8 shows that the injected slug is already very diffused about 20 hours after the start of the injection. This fact confirms the very fast dynamics of the system. Again ERT and GPR multi-

offset gathers consistently show similar features, even though the ERT image is neater. In Fig. 9, both ERT and multi-offset gathers show the onset of what appears as a new pulse of injection: this is due to very heavy rainfall that occurred during the night of July 7, and freely and quickly infiltrated through the open trench.

Water infiltration can also be effectively tracked by GPR zero-offset profiles: in Fig. 10, the six available profiles are shown (already converted into moisture content using equation (2)). Here too the very fast infiltration and diffusion of the injected water can be observed. The vertical position of the centre of mass of the injected water (the red arrows in Fig. 10) can be tracked up to two days after the injection, even though the accuracy of this measurement clearly becomes poorer as time progresses. zero-offset-profile data also show the very fast rise of the water table (half-a-metre in only four days) as a result of regional irrigation during this central summer period.

Unsaturated flow modelling and comparison with field data

The geophysical data acquired during water injection, and converted to a quantitative estimate of volumetric moisture content, can be used to calibrate a variably saturated flow model in order to identify key sediment parameters, such as hydraulic conductivity (see Fig. 1 and e.g. Binley *et al*. 2002b; Cassiani *et al*. 2004; Cassiani and Binley 2005). Generally, the modelling of water flow in the unsaturated zone is represented by Richards' equation, which in three dimensions reads

$$\frac{\partial}{\partial x}\left[K_{\mathrm{H}}(h)\frac{\partial h}{\partial x}\right]+\frac{\partial}{\partial y}\left[K_{\mathrm{H}}(h)\frac{\partial h}{\partial y}\right]+\frac{\partial}{\partial z}\left[K_{\mathrm{V}}(h)\frac{\partial (h+z)}{\partial z}\right]=\frac{\partial \theta}{\partial t}, \qquad (3)$$

where z [L] is elevation, h [L] is pressure head, θ [-] is volumetric moisture content, $K_{\mathrm{H}}(h)$ and $K_{\mathrm{V}}(h)$ are, respectively, the horizontal and vertical unsaturated hydraulic conductivity [L/T] as a function of pressure head. Note that equation (3) assumes that x, y and z are the principal direction of the (possibly anisotropic) hydraulic conductivity tensor. The system is isotropic if $K_{\mathrm{H}}(h)=K_{\mathrm{V}}(h)=K(h)$. Equation (3) must be supplemented with relevant constitutive models linking h, θ and K. The most important parameter is the saturated hydraulic conductivity K_{s} [L/T], which is the upper limit of $K(h)$ occurring at full saturation (h=0). K_{s} has a critical role in the dynamics of the vadose zone; in particular, it controls the speed of water infiltration, i.e. the impact of gravitational forces on unsaturated water flow. For this reason, it is possible to calibrate a model with respect to K_{s} on the basis of the sinking process of the water bulb during a water-injection experiment (Binley *et al*. 2002b). The data necessary for this calibration can be obtained, in the case of our experiment, from zero-offset profiles (Fig. 10) and ERT difference images (Figs 6–9).

A 3D unsaturated flow model was built using the FEMWATER model (Lin *et al.* 1997), which solves equation (3) using a finite-element formulation. The vadose zone underlying the Gorgonzola site to a depth of 19 m was discretized using a vertical spacing of 25 cm, with 37004 prism elements and 21172 nodes. The 3D mesh represents only one-quarter of the site, thanks to symmetry around the trench. Injection was simulated as a second-type boundary condition at the trench bottom, honouring the measured flow rates. No flow boundary conditions were applied to the model sides, while a water-table condition was set at the model bottom. Initial conditions in the model were set to correspond to gravity-drained conditions, assuming that this condition corresponds to what is observed by the long-term monitoring of natu-

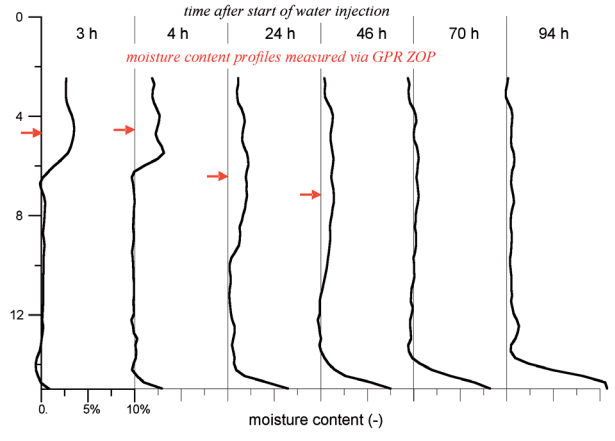

FIGURE 10

Moisture-content excess with respect to background (i.e. before water injection in the trench), as a function of depth, derived from zero-offset profile (ZOP) GPR measurements at six instants in time after the start of injection (given in hours). The arrows indicate the vertical location of the centre of mass of the injected water. Note the rise in the water table in the deeper part of the profile, as a consequence of regional irrigation.

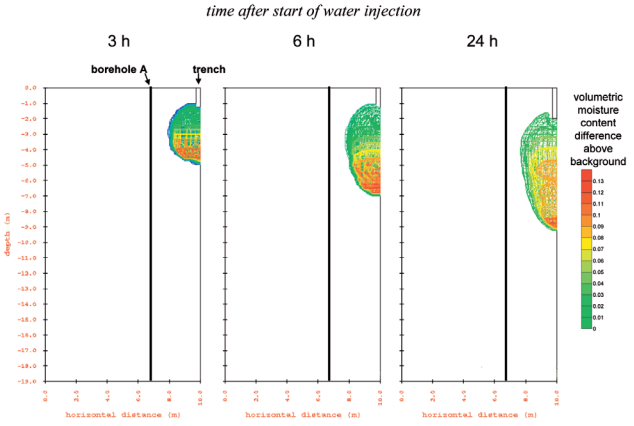

FIGURE 11

Moisture-content difference with respect to background as simulated using a 3D unsaturated flow model based on FEMWATER (Lin *et al*. 1997), using *isotropic* saturated hydraulic conductivity equal to 5 m/d. The model simulates only one-quarter of the full 3D space, due to symmetry.

ral conditions (Fig. 3). This assumption was confirmed by laboratory measurements of residual moisture content at a number of locations along the extracted core, corresponding well to the observed moisture content profiles in Fig. 3. Porosity for the entire model was set equal to 0.28, consistent with the observed moisture content below the water table (see Fig. 3). A van Genuchten parametrization was adopted for unsaturated flow properties, choosing parameters representative of a coarse sand/gravel, i.e. $n = 2.2$ and $\alpha = 2$ m^{-1}, for the entire model. Only the saturated hydraulic conductivity Ks was modified by trial and error to match field data.

A first set of simulations were conducted assuming that the system is isotropic. An example of moisture content excess with respect to background is shown in Fig. 11 for one of these cases (K_s = 5 m/d). The corresponding vertical moisture-content profiles obtained by averaging the modelled 3D moisture-content distribution along the horizontal direction between boreholes A and B (mimicking the zero-offset-profile acquisition) is shown in Fig. 12, together with the computed vertical location of the centre of mass. Figure 13 shows the results of isotropic model calibration in terms of depth of the centre of mass of the injected water. Note that zero-offset-profile and ERT data are consistent in terms of centre-of-mass sinking, and allow for a fairly precise calibration of the flow model. If a value for K_s that is consistent with the field-measured (horizontal) hydraulic conductivity (36 m/d) is adopted, two inconsistencies are noted with respect to field moisture-content distribution: (1) the centre of mass sinks exceedingly fast in the model and (2) the water slug disappears very quickly (in about 1 day) as a consequence of the fast diffusion allowed by a high K_s. Several other values for K_s were adopted (see Fig. 13) spanning about one order of magnitude (2.5–36 m/d). Note that the field-measured centre-of-mass motion constrains the range of isotropic K_s very strictly; K_s was ultimately estimated to lie between 5 and 10 m/d. In spite of this clear result, the water volume 'seen' in the simulations (see Fig. 12) is considerably larger than that measured by zero-offset profiles (Fig. 10). At the same time, the horizontal spread of simulated water slugs (e.g. Fig. 11) does not resemble the appearance of measured ERT and GPR multi0-offset-gather data (Figs 6–8 in particular). Both factors seem to indicate that there should be a larger spread of moisture content away from the centre of mass, particularly in the horizontal direction.

In order to resolve the inconsistency noted in the simulations above, we also ran a set of anisotropic models, having horizontal hydraulic conductivity greater than the vertical value. In order to constrain the number of parameters for model calibration, we assumed as known the value of the horizontal hydraulic conductivity (K_{sH} =36 m/d, as measured by the Lefranc test) and allowed only the anisotropy ratio of horizontal to vertical conductivity ($\alpha = K_{sH} / K_{sV}$) to vary. The corresponding time evolution of the centre of mass of the injected water is shown in Fig. 14. A value of α around 2 is suitable to match the field data with the same degree of accuracy as isotropic models hav-

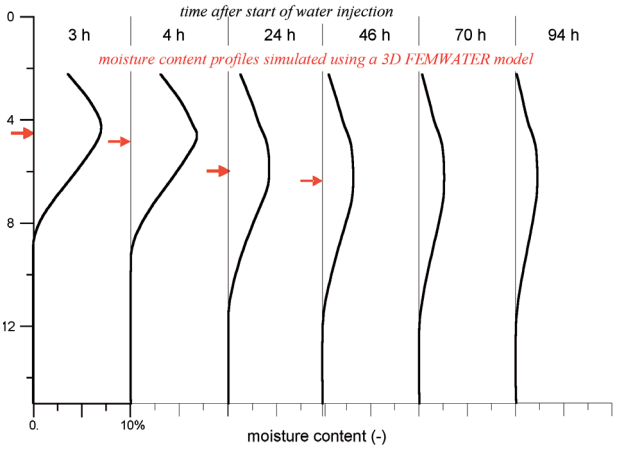

FIGURE 12
Vertical profiles of moisture-content excess with respect to background (i.e. before water injection in the trench) as a function of depth, derived from the 3D unsaturated flow model based on FEMWATER at six instants in time after the end of injection (given in hours). The profiles are obtained by horizontal averaging along straight lines between boreholes A and B. The case presented here utilizes *isotropic* saturated hydraulic conductivity equal to 5 m/d. The arrows indicate the vertical location of the centre of mass of injected water.

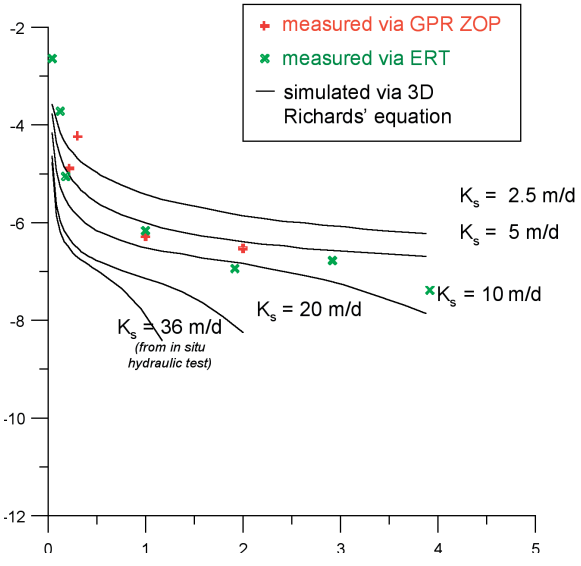

FIGURE 13
Centre-of-mass vertical motion as computed by 3D infiltration flow simulations (using FEMWATER) using *isotropic* hydraulic conductivity, compared with the centre-of-mass motion derived from ZOP data (Fig. 10) and from ERT difference resistivity images (Figs 6–9). Five values of saturated hydraulic conductivity (K_s) of the subsoil were used and provide different results. K_s=36 m/d is the value obtained from *in-situ* testing during drilling. The curves derived from simulation are interrupted when the injected water slug is too diffused to yield reliable estimates of the centre of mass.

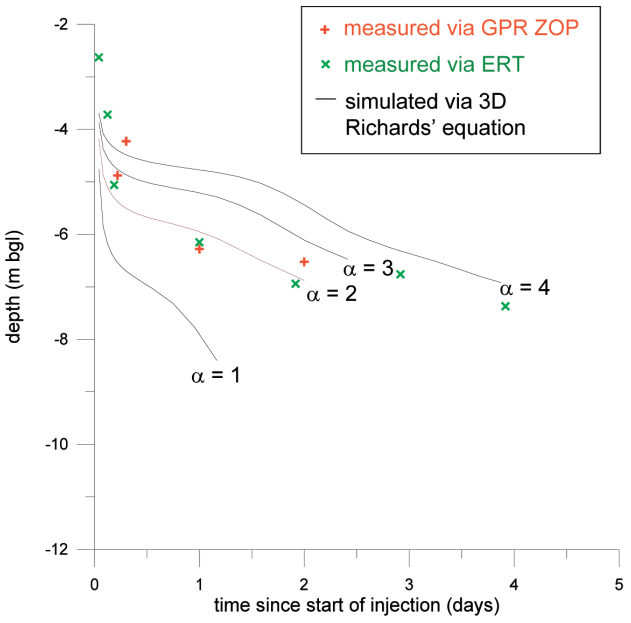

FIGURE 14
Centre-of-mass vertical motion as computed by 3D infiltration flow simulations (using FEMWATER) compared with the centre-of-mass motion derived from ZOP data (Fig. 10) and from ERT difference resistivity images (Figs 6–9). The 3D flow model is here assumed to be *anisotropic*, with horizontal conductivity of 36 m/d, and with varying vertical conductivity according to the horizontal/vertical ratio α. The curves derived from simulation are interrupted when the injected water slug is too diffused to yield reliable estimates of the centre of mass.

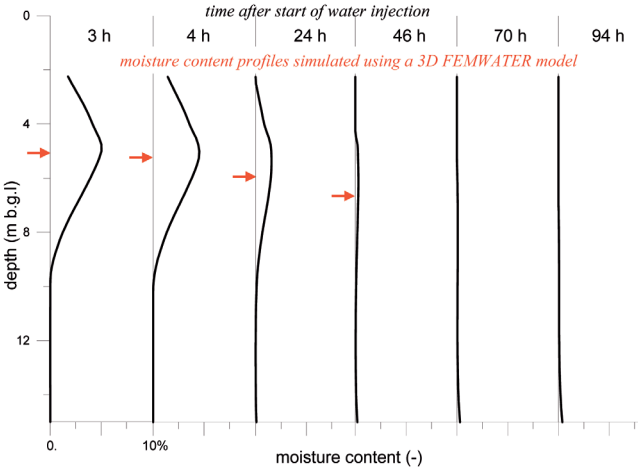

FIGURE 15
Vertical profiles of moisture-content excess with respect to background (i.e. before water injection in the trench) as a function of depth, derived from the 3D unsaturated flow model based on FEMWATER at six instants in time after the end of injection (given in hours). The profiles are obtained by horizontal averaging along straight lines between boreholes A and B. The case presented here utilizes *anisotropic* saturated hydraulic conductivity, with horizontal conductivity equal to 36 m/d and vertical conductivity equal to 18 m/d (α = 2). The arrows indicate the vertical location of the centre of mass of injected water.

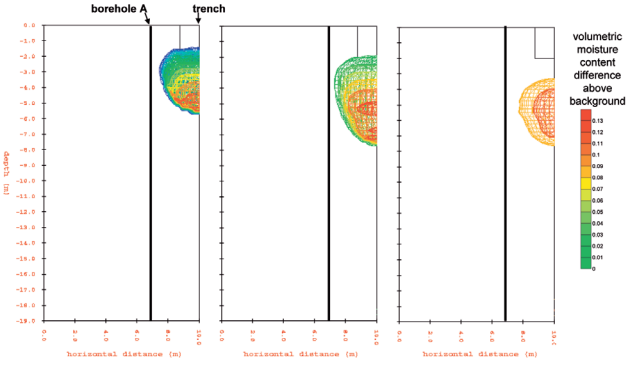

FIGURE 16
Moisture-content difference with respect to background as simulated using a 3D unsaturated flow model based on FEMWATER using *anisotropic* saturated conductivity, with horizontal conductivity equal to 36 m/d and vertical conductivity equal to 18 m/d (α = 2). The model simulates only one-quarter of the full 3D space, due to symmetry.

ing K_s = 5–10 m/d (see Fig. 13). However, the anisotropic models also have the advantage of a more favourable match of excess moisture content with respect to field data (see Fig. 15, compared with Figs 12 and 10). In addition, the appearance of the water slug in the model (Fig. 16) is more consistent with the observed lateral spread in ERT and multi-offset-gather images (Figs 6–9). We can conclude that an anisotropic hydraulic conductivity field with K_{sH} =36 m/d, K_{sV} =18 m/d can be considered as the best estimate at the scale of cross-hole data measurement (~10 m).

4 DISCUSSION AND CONCLUSIONS

The use of non-invasive cross-hole GPR and ERT data to calibrate unsaturated flow models is an invaluable tool to derive unsaturated hydraulic parameters under *in-situ* conditions. It is extremely difficult to derive similar estimates in the unsaturated zone from direct measurements, which are heavily affected by soil disturbance and other errors (e.g. smearing of fine soil fractions on the borehole wall in Lefranc tests).

The water-injection experiment conducted at the Gorgonzola test site proves that fast infiltration in permeable Quaternary sediments can be monitored accurately by both borehole ERT and GPR in time-lapse mode. While the methodology presented in this paper is similar to that of Binley *et al*. (2002b), Quaternary sediments are a much faster system than the UK Permo-Triassic sandstone discussed by Binley *et al*. (2002b). Hydraulic conductivity here is two orders of magnitude larger. This fact implies that a faster and potentially less accurate monitoring system must be set in place. Our

work proves that, in spite of these practical difficulties, the collected data still allow for a precise calibration of *in-situ* hydraulic conductivity. Note that Quaternary sediments are very common and are widely studied for both water-quality and water-quantity problems.

The system described here is also more complex than the one described by Binley *et al.* (2002b). Some degree of vertical layering is evident from the residual moisture-content profiles (Fig. 3). As a consequence, the system is likely to have a certain degree of vertical/horizontal anisotropy. In fact, a joint consideration of (1) vertical motion of the centre of mass of the water and (2) water-mass balance between data and simulations allows for a more complete picture to be drawn. In this specific case, this joint analysis leads to the conclusion that the system is anisotropic. Note also that the values of horizontal (36 m/d) and vertical (18 m/d) hydraulic conductivity, estimated using an anisotropic model, are both considerably larger than the best estimate obtained by isotropic model calibration (5–10 m/d), based solely on the centre-of-mass motion.

In the example presented, only limited spatial information could be derived from non-invasive monitoring because of the relatively small volume of injected water, which effectively invades only the upper part of the soil profile (no deeper than 6 m) before diffusing below detection. A large water volume should be injected in a possible repeat of the experiment. Moreover, the very fast dynamics of the system would require more frequent measurements, particularly in the early time of injection. Such frequent measurements can only be possible using a zero-offset-profile acquisition scheme, which requires only a few minutes for each survey. While zero-offset-profile surveys clearly limit our considerations mainly to vertical migration, indications of overall mass balance and possibly of anisotropy (in terms of lateral spread of the slug) can still be obtained as shown by the results of this paper.

Further refinements of the proposed techniques should be directed towards quantitatively integrating ERT and GPR to yield a single best image of the flow dynamics. Such integration could effectively take advantage of the complementary spatial resolution characteristics of both borehole tomography methods.

ACKNOWLEDGEMENTS

We acknowledge the financial support from the Consorzio Industriale di Gorgonzola/Pessano con Bornago that made this study possible. The thorough analysis and useful suggestions of two anonymous reviewers are gratefully acknowledged. We also thank Nicoletta Fusi for help with laboratory analysis.

REFERENCES

Alumbaugh D., Chang P.Y., Paprock L. I., Brainard I.R., Glass R.J. and Rautman C.A. 2002. Estimating moisture contents in the vadose zone using cross-borehole ground penetrating radar: A study of accuracy and repeatability. *Water Resources Research* **38** (12), 1309, doi: 10.1029/2001 WR000754.

Annan A.P. 2005. *GPR Methods for Hydrogeological Studies*. Springer Hydrogeophysics Series: Water Science and Technology Library **50** (eds Y. Rubin and S.S. Hubbard).

Archie G.E. 1942.

Binley A.M., Cassiani G., Middleton R., and Winship P. 2002b. Vadose zone flow model parameterisation using cross-borehole radar and resistivity imaging. *Journal of Hydrology* **267**(3–4), 147–159.

Bing Z. and Greenhalgh S.A. 2000. Cross-hole resistivity tomography using different electrode configurations. *Geophysical Prospecting* **48**, 887–912.

Binley A.M., Henry-Poulter S. and Shaw B. 1996. Examination of solute transport in an undisturbed soil column using electrical resistance tomography. *Water Resources Research* **32** (4), 763–770.

Binley A.M. and Kemna A. 2005. *DC Resistivity and Induced Polarization Methods*. Springer Hydrogeophysics Series: Water Science and Technology Library **50**, (eds Y. Rubin and S.S. Hubbard).

Binley A.M., Winship P., Middleton R., Pokar M. and West J. 2001. High resolution characterization of vadose zone dynamics using cross-borehole radar. *Water Resources Research* **37**(11), 2639–2652.

Binley A.M., Winship P., West L.J., Pokar M. and Middleton R. 2002a. Seasonal variation of moisture content in unsaturated sandstone inferred from borehole radar and resistivity profiles. *Journal of Hydrology* **267**(3–4), 160–172.

Cassiani G. and Binley A.M. 2005. Modeling unsaturated flow in a layered formation under quasi-steady state conditions using geophysical data constraints. *Advances in Water Resources* **28**(5), 467–477.

Cassiani G., Binley A.M. and Ferré T.P.A. 2006a. *Unsaturated Zone Processes*. Applied Hydrogeophysics (eds H. Vereecken *et al.*), IV Earth and Environmental Sciences, Nato Science Series.

Cassiani G., Bruno V., Villa A., Fusi N. and Binley A.M. 2006c. A saline tracer test monitored via time-lapse surface electrical resistivity tomography. *Journal of Applied Geophysics* **59**(3), 244–259.

Cassiani G., Strobbia C. and Gallotti L. 2004. Vertical radar profiles for the characterization of deep vadose zones. *Vadose Zone Journal* **3**, 1093–1115.

Cassiani G., Strobbia C., Giustiniani M., Fusi N., Crosta G.B. and Frattini P. 2006b. Monitoring of hydrological hillslope processes via time-lapse ground-penetrating radar. *Bollettino di Geofisica Teorica ed Applicata* **47** (1–2), 125–144.

Chan C. Y. and Knight R. J. 1999. Determining water content from dielectric measurements in layered materials. *Water Resources Research* **35**(1), 85–93.

Chelidze T.L. and Gueguen Y. 1999. Electrical spectroscopy of porous rocks: a review- I. Theoretical models. *Geophysical Journal International* **137**(1), 1–15.

Constable S.C., Parker R.L. and Constable C.G. 1987. Occam's inversion: A practical algorithm for generating smooth models from electromagnetic sounding data. *Geophysics* **52**, 289–300.

Daily W.D., Lin W. and Buscheck T. 1987. Hydrological properties of TOPOPAH Spring tuff – Laboratory measurements. *Journal of Geophysical Research* **92**, 7854–7864.

Daily W., Ramirez A. and Binley A. 2004b. Remote monitoring of leaks in storage tanks using electrical resistance tomography: application at the Hanford site. *Journal of Environmental and Engineering Geophysics* **9**(1), 11–24.

Daily W., Ramirez A., Binley A. and LaBrecque D. 2004a. Electrical resistance tomography. *The Leading Edge* **23**(5), 438–442.

Daily W., Ramirez A., Binley A. and LaBrecque D. 2005. *Electrical Resistance Tomography - Theory and Practice.* Near-Surface Geophysics, Investigations in Geophysics **13**, (ed. D.K. Butler), pp. 525–550. Society of Exploration Geophysicists Monographs.

Daily W.D., Ramirez A.L., LaBrecque D.J and Nitao J. 1992. Electrical resistivity tomography of vadose water movement. *Water Resources Research* **28**(5), 1429–1442.

Daniels J.J., Allred B., Binley A., LaBrecque D. and Alumbaugh D. 2005. *Hydrogeophysical Case Studies in the Vadose Zone*. Springer Hydrogeophysics Series: Water Science and Technology Library **50** (eds Y. Rubin Y. and S.S. Hubbard).

Day-Lewis F.D. and. Lane J.W Jr. 2004. Assessing the resolution-dependent utility of tomograms for geostatistics. *Geophysical Research Letters* **31**, L07503, doi:10.1029/2004GL019617.

Day-Lewis F., Singha K. and Binley A. 2005. On the limitations of applying petrophysical models to tomograms:a comparison of correlation loss for cross-hole electrical-resistivity and radar tomography. *Journal of Geophysical Research* **110** (B8), B08206, 10.1029/2004JB003569.

Eppstein M.J. and Dougherty D.E. 1998. Efficient three-dimensional data inversion: Soil characterization and moisture monitoring from cross-well ground-penetrating radar at the Vermont test site. *Water Resources Research* **34**(8), 1889–1900.

Flury M., Fluhler H., Jury W.A. and Leuenberger J. 1994. Susceptibility of soils to preferential flow of water: A field study. *Water Resources Research* **30**(7), 1945–1954.

French H.K., Hardbattle C., Binley A., Winship P. and Jakobsen L. 2002. Monitoring snowmelt induced unsaturated flow and transport using electrical resistivity tomography. *Journal of Hydrology* **267**(3–4), 273–284.

Grote K., Hubbard S. and Rubin Y. 2003. Field-scale estimation of volumetric water content using ground-penetrating-radar wave techniques. *Water Resources Research* **39**(11), 1321, doi:10.1029/2003WR002045.

Hubbard S.S., Peterson J.E.Jr., Majer E.L., Zawislanski P.T., Williams K.H., Roberts J. and Wobber F. 1997. Estimation of permeable pathways and water content using tomographic radar data. *The Leading Edge* **16**(11), 1623–1628**.**

Huisman J.A., Hubbard S.S., Redman J.D. and Annan A.P. 2003. Measuring soil water content with Ground Penetrating Radar: a review. *Vadose Zone Journal* **2**, 477–491.

Huisman J.A., Snepvangers J.J.J.C., Bouten W. and Heuvelink G.B.M. 2002, Mapping spatial variation of surface soil water content: comparison of ground-penetrating radar and time domain reflectometry. *Journal of Hydrology* **269**, 194–207.

Huisman J.A., Sperl C., Bouten W. and Verstraten J.M. 2001. Soil water content measurements at different scales: Accuracy of time domain reflectometry and ground-penetrating radar. *Journal of Hydrology* **245**(1–4)**,** 48–58.

Irving J.D. and Knight R.J. 2005. Effects of antennas on velocity estimates obtained from cross-hole GPR data. *Geophysics* **70**(5) K39–K42, 10.1190/1.2049349.

Jackson M.J. and Tweeton D.R. 1994. *MIGRATOM - Geophysical tomography using wavefront migration and fuzzy constraints*. USBM Report of Investigation 9497, 35.

Kemna A. 2000. *Tomographic inversion of complex resistivity: theory and application*. *PhD dissertation, University of Bochum, Germany*.

Kemna A., Vanderborght J., Kulessa B. and Vereecken H. 2002. Imaging and characterisation of subsurface solute transport using electrical resistivity tomography (ERT) and equivalent transport models. *Journal of Hydrology* **267**(3–4), 125–146.

LaBrecque D.J., Miletto M., Daily W.D., Ramirez A.L.and Owen E. 1996. The effects of noise on Occam's inversion of resistivity tomography data. *Geophysics* **61**, 538–548.

LaBrecque D.J. and Yang X. 2000. Difference inversion of ERT data: a fast inversion method for 3-D in-situ monitoring. *Proceedings of Symposium on Applied Geophysics, Engineering and Environmental Problems,* pp.723–732. Environmental and Engineering Geophysical Society.

Lesmes D.P. and Friedman S.P. 2005. Relationships between the electrical and hydrogeological properties of rocks and soils. In: *Hydrogeophysics* (eds Y. Rubin and S.S. Hubbard), ch. 4, pp. 87–128. Springer, Dordrecht, The Netherlands.

Lin H.J., Richards D.R., Talbot C.A., Yeh G.T., Cheng J. and Cheng H. 1997. *FEMWATER: A three-dimensional finite element computer model for simulating density-dependent flow and transport in variably saturated media.* US Army Corps of Engineers and Pennsylvania State, University Technical Report, CHL-97-12.

Park S. 1998. Fluid migration in the vadose zone from 3-D inversion of resistivity monitoring data. *Geophysics* **63**, 41–51.

Peterson J.E.Jr. 2001. Pre-inversion processing and analysis of tomographic radar 752 data. *Journal of Environmental and Engineering Geophysics* **6**, 1–18.

Ramirez A., Daily W., Binley A., LaBrecque D. and Roelant D. 1996. Detection of leaks in underground storage tanks using electrical resistance methods. *Journal of Environmental and Engineering Geophysics* **1**, 189–203.

Roth K., Schulin R., Fluhler H. and Hattinger W. 1990. Calibration of time domain reflectometry for water content measurements using a composite dielectric approach. *Water Resources Research* **26**(10), 2267–2273.

Rucker D.F. and Ferré T.P.A. 2004. Correcting water content measurements errors associated with critically refracted first arrivals on zero offset profiling borehole ground penetrating radar profiles. *Vadose Zone Journal* **3**(1), 278–287.

Singha K. and Gorelick S.M. 2005. Saline tracer visualized with three-dimensional electrical resistivity tomography: Field-scale spatial moment analysis. *Water Resources Research* **41** W05023, doi:10.1029/2004WR003460.

Slater L., Binley A., Daily W.and Johnson R. 2000. Cross-hole electrical imaging of a controlled saline tracer injection. *Journal of Applied Geophysics* **44**(2–3), 85–102.

Slater L. and Lesmes D.P. 2002. Electrical-hydraulic relationships observed for unconsolidated sediments, *Water Resources Research* **38**(10), 1213 1029/2001WR001075.

Slater L., Versteeg R., Binley A., Cassiani G., Birken R.and Sandberg S. 2002. A 3D ERT study of solute transport in a large experimental tank. *Journal of Applied Geophysics* **49**, 211–229.

Slater L., Zaidman M.D., Binley A.M. and West L.J. 1997. Electrical imaging of saline tracer migration for the investigation of unsaturated zone transport mechanisms. *Hydrology and Earth System Sciences* **1,** 291–302.

Topp G.C., Davis J.L. and Annan A.P. 1980. Electromagnetic determination of soil water content: measurements in coaxial transmission lines. *Water Resources Research* **16**, 574–582.

Vanderborght J., Kemna A., Hardelauf H. and Vereecken H. 2005. Potential of electrical resistivity tomography to infer aquifer transport characteristic from tracer studies: A synthetic case study. *Water Resources Research* **41**, 06013, doi:10.1029/2004WR003774, 23.

van Overmeeren R.A., Sariowan S.V. and Gehrels J.C. 1997. Ground penetrating radar for determining volumetric soil water content: Results of comparative measurements at two test sites. *Journal of Hydrology* **197**(1-4), 316–338.

Zaidman M.D., Middleton R.T., West L.J. and Binley A.M. 1999. Geophysical investigation of unsaturated zone transport in the Chalk in Yorkshire. *Quarterly Journal of Engineering Geology and Hydrogeology* **32**(2), 185–198.